



Measurement Report: Diurnal Variability of NO₂ and HCHO Lower Tropospheric Vertical Profiles in Southeastern Los Angeles

Peter K. Peterson¹, Lisa F. Hernandez¹, Leslie Tanaka¹, and Alejandro Dunnick¹

¹Department of Chemistry, Whittier College, Whittier, CA, USA

Correspondence: Peter K. Peterson (ppeterso@whittier.edu)

Abstract. Ground level ozone in excess of United States ambient air quality standards remains a prevalent issue across Southern California, particularly in the summer months. To improve our understanding of the vertical distribution of ozone precursors in southern California, we used ground-based MAX-DOAS measurements in Whittier CA to simultaneously retrieve both near-surface mole fractions and vertical column densities of both NO₂ and HCHO. Ratios of HCHO to NO₂, commonly referred to as FNR, derived from satellite-based measurements are used to diagnose ozone production chemistry over regions without consistent surface based measurements. While vertical column densities of NO₂ are well correlated with TROPOMI observations over the study period (R=0.73), HCHO VCDs and FNRs derived from MAX-DOAS observations are less well correlated (R=0.47 and 0.38, respectively). These observations also show differing diurnal cycles between near surface mixing ratios and vertical column densities due to variability in the vertical profile that will be increasingly critical to understand given the ongoing shift from sun synchronous to geostationary satellite observations. Using ground-based measurements, we determine FNRs using both surface mole fractions and vertical column densities, finding FNRs derived from surface mole fractions are generally lower than those derived from column based measurements. Evaluating ozone exceedance probability as a function of FNR for both quantities suggests the transition between a VOC limited and NO_x limited regimes may begin at lower FNR values than those derived from satellite based measurements in East LA. We find these differences in FNR derived from ground based and satellite based measurements are driven by variability in the vertical distribution of HCHO. These impacts are most pronounced in late afternoon, when ozone exceedances are most prevalent.

1 Introduction

While the atmospheric chemistry over Los Angeles has been extensively studied with both long term measurements and dedicated intensive field campaigns (e.g. Hering and Blumenthal, 1989; Jacob et al., 2010; Ryerson et al., 2013; Nussbaumer et al., 2023) ozone mole fractions in excess of United States ambient air quality standard (NAAQS) of 70 nmol mol⁻¹ remain a frequent issue across the region, particularly at warmer temperatures (Pusede et al., 2015), pointing to a continued need for measurements of ozone and its precursors in Southern California.

Ozone production is dependent in a non-linear fashion on both nitrogen oxides (NO_x≡NO + NO₂) and volatile organic compounds (VOCs) (Haagen-Smit, 1952; Sillman et al., 1990). NO_x is emitted via both natural sources (e.g. wildfires, lightning) and anthropogenic sources, primarily via combustion. VOCs have a variety of sources including biogenic emissions, wildfires,



and anthropogenic emissions. Formaldehyde is often used in studies as a proxy for VOCs due to it being a common product of VOC oxidation reactions (Millet et al., 2006) and ability to be detected with spectroscopic and remote sensing techniques (e.g. Duncan et al., 2010).

Satellite based measurements of ozone precursors that absorb strongly in the ultraviolet such as NO_2 and HCHO have been used to understand ozone production chemistry over wide regions, particularly those without robust surface monitoring networks (e.g. Martin et al., 2004; Duncan et al., 2010; Jin et al., 2017, 2020; Souri et al., 2020). However, the relationship between the retrieved vertical column densities and near surface mixing ratios more relevant to human health is not straight forward and complicates the use of these data to inform interventions to improve regional air quality (e.g. Schroeder et al., 2017). In addition to direct measurements of NO_2 and HCHO, ratios of HCHO to NO_2 (FNR) obtained via remote sensing have been explored as a potential diagnostic tool for whether ozone formation chemistry is NO_x limited or NO_x saturated (e.g. Martin et al., 2004; Duncan et al., 2010; Jin et al., 2017, 2020; Souri et al., 2020). The use of these column measurements and derived ratios to examine near-surface ozone formation chemistry is complicated by variations in the trace gas vertical profile that confound the relationship between the satellite observed vertical column densities and ground level pollutant concentrations which are the target of policy efforts to improve air quality. In particular, results from the DISCOVER-AQ campaign showed that variations in the HCHO and NO_2 vertical profiles lead to ratios of HCHO/ NO_2 columns that do not reflect ozone production conditions at ground level (Schroeder et al., 2017). Inter-comparisons with ground based measurements to try and improve our understanding of these impacts to date have only been undertaken at times centered around a once daily satellite overpass. The ongoing shift from sun synchronous to geostationary satellite observations will require a better understanding of the diurnal behavior of vertical profiles of these trace gases to interpret satellite based column measurements.

Multiple Axis Differential Absorption Spectroscopy (MAX-DOAS) is frequently used to provide information on both near surface and total column amounts of HCHO and NO_2 concurrently with high temporal resolution during daylight hours and is well suited to provide observational data on how the relationship between these two quantities varies throughout the day. In this work we present two years of vertically resolved measurements of NO_2 and HCHO measurements in southeastern Los Angeles county and their relationship with local ozone conditions. These measurements are the first vertically resolved characterization of these two ozone precursors in southeastern Los Angeles county, improving our understanding of the diurnal variation in ozone precursors and resulting ozone pollution in this part of Southern California.

2 Methods

2.1 MAX-DOAS Measurements

Multiple axis differential optical absorption spectroscopy (MAX-DOAS) (Hönninger et al., 2004) measurements were made using an Airyx SkySpec-Compact-150 system on the Whittier College campus from 26 March 2020 to 26 May 2022. Whittier College is located approximately 15 km southeast of downtown Los Angeles directly west of the Puente Hills (Fig. 1). The view azimuth of the instrument was 180 degrees east of north, and is shown in Fig. 1 with a black line. Solar spectra were obtained at 1,2,3,5,10,20,40, and 90 degree elevation angles, with one elevation scan taking place over approximately 10 minutes.

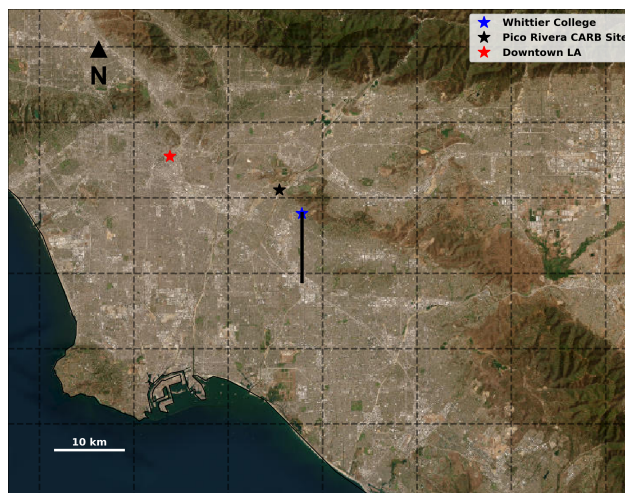


Figure 1. Map of the area surrounding Whittier College (Esri, 2024). The location of Whittier College, where the MAX-DOAS measurements took place, is indicated with a blue star. The black line extending from the blue star indicates the view azimuth and approximate horizontal path length of the DOAS observations. The California Air Resources Board site with in situ measurements used in this study is indicated with a black star.

Table 1. Median dSCD fitting errors compared to data from standard instruments deployed during the CINDI-2 campaign (Kreher et al., 2020).

Data Product	This study	Standard Instruments (Kreher et al. (2020))
NO ₂ (UV)	8.6×10^{14} (molec cm ⁻²)	1×10^{15} (molec cm ⁻²)
HCHO	1.9×10^{15} (molec cm ⁻²)	8×10^{15} (molec cm ⁻²)
O ₄ (UV)	4.1×10^{41} (molec ² cm ⁻⁵)	8×10^{41} (molec ² cm ⁻⁵)

DOAS fitting for O₄, NO₂, and HCHO was undertaken using QDOAS (Fayt et al., 2011) following the recommendations
60 from the CINDI-2 intercomparison campaign outlined in Kreher et al. (2020) (Fit windows: NO₂, O₄: 338–370 nm, HCHO:
324.5–359 nm), with exception of the use of a zenith reference spectrum for each elevation scan to minimize the influence of
stratospheric trace gases on the spectral fitting. Fits with an RMS value less than 0.001 were not included in further analysis.
Typical differential slant column uncertainties, characterized by median fitting errors, shown in Table 1. Cloud screening of
these data was done based on the measured colour index (I_{330}/I_{404}) using methods detailed in Wagner et al. (2016). This cloud
65 screening removed 8.1% of the data set overall and had a distinct seasonal cycle, shown in Fig. 2, resulting in a dataset that is
overly weighted toward spring and summer observations when clear skies were more prevalent. The remaining cloud screened
measurements were then used to retrieve vertical profiles of NO₂ and HCHO concentrations averaged over 100 m layers up to
an altitude of 4 km, providing vertical profile information for NO₂ and HCHO with 30 min temporal resolution.

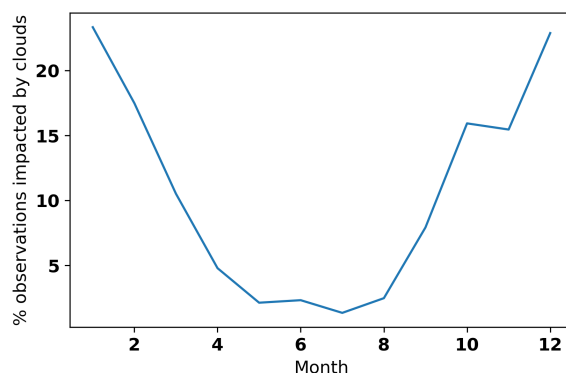


Figure 2. The percentage of data removed by cloud screening as a function of month. This figure illustrates the larger impact of cloud screening on observations during the winter months.

The retrieval of trace gas vertical profiles from MAX-DOAS slant column densities was performed using HEIPRO (Yilmaz, 2012). The retrieval is a two step process completed using optimal estimation (Rodgers, 2000; Wagner et al., 2004; Frieß et al., 2006). First, the aerosol particle extinction profile is retrieved using slant column density measurements of O_4 , which has a known vertical profile dependent only on temperature and pressure, with the radiative transfer model SCIATRAN (Rozanov et al., 2005) serving as the forward model. For the aerosol extinction profile retrieval, the a priori consisted of an exponentially decaying profile with a scale height of 0.5 km and an aerosol optical depth (AOD) determined by the median measured AOD at the CalTech AERONET site over the measurement period. Similarly, the angstrom exponent (1.23), and phase function (0.70) were also determined using median measured values from the CalTech AERONET site. The surface albedo was assumed to be 0.1 and the aerosol single scattering albedo was assumed to be 0.92 based on measurements during CALNEX (Thompson et al., 2012).

The trace gas retrieval is done similarly using the retrieved aerosol extinction profile as input for the forward model. For NO_2 , the a priori was an exponentially decaying profile with a 0.5 km scale height and a value in the lowest layer of 14 nmol mol^{-1} . This value was based on the median of in situ NO_2 measurements during this time period at the California Air Resources Board site in Pico Rivera, 5 km north of the college. For CH_2O , the a priori was an exponentially decaying profile with a 500 m scale height and a value in the lowest layer of 6 nmol mol^{-1} based on measurements during the 2010 CalNex campaign (Warneke et al., 2011).

While the trace gas profiles are typically retrieved on a high spatial resolution grid, in this case every 100 m up to 4 km, this is an over-representation of the actual information content of the original measurements with 40 parameters being retrieved from 7 measurements. Thus, it is desirable to reduce the retrieved profiles to more robust quantities that accurately reflect the information content of the measurements as well as facilitate analysis of long term measurements (Payne et al., 2009; Peterson et al., 2015). With ground-based MAX-DOAS, which is most sensitive near the surface, we reduced the retrieved profiles to a near-surface mole fractions and a lower tropospheric vertical column density (LT-VCD) to emphasize that the retrieved

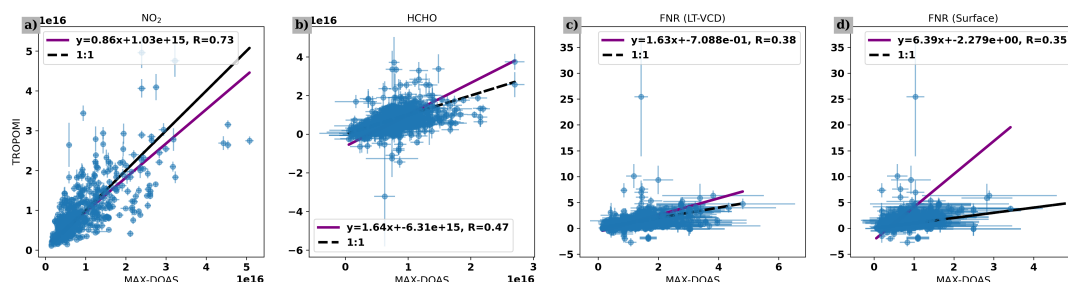


Figure 3. a) Correlation of hourly averaged MAX-DOAS NO₂ retrievals with tropospheric columns retrieved from TROPOMI. b) Correlation of hourly averaged MAX-DOAS HCHO retrievals with tropospheric columns retrieved from TROPOMI. c) Correlation of hourly averaged MAX-DOAS LT-VCD based FNRs with those calculated using tropospheric columns retrieved from TROPOMI. d) Correlation of hourly averaged MAX-DOAS surface based FNRs with those calculated using tropospheric columns retrieved from TROPOMI. The purple lines show the orthogonal distance regression, while the black dashed lines shows the 1:1 relationship. Uncertainties for both retrievals are shown in blue.

columns do not necessarily reflect the full tropospheric column (Peterson et al., 2015). Over the course of the study, 93% of NO₂ measurements and 94% of HCHO measurements had more than two degrees of freedom, as determined from the retrieval averaging kernel matrix, indicating that both these quantities could be reliably retrieved from the dSCD measurements. To characterize variability in the vertical distribution of the trace gas of interest, we also calculated the fraction of the retrieved column in the lowest 200 m, which we refer to as the f₂₀₀ (Peterson et al., 2015). The cloud screened data set consists of 5,790 30 min observations of near-surface mole fractions, LT-VCDs, and f₂₀₀s for both NO₂ and HCHO.

2.2 Complementary Data

Hourly O₃ and temperature measurements were obtained from the Pico Rivera # 2 South Coast Air Quality Measurement District (SCAQMD) site 5 km northeast of the college (Fig. 1). SCAQMD utilizes Teledyne Advance Pollution Instrumentation, Inc Model T400 instruments to measure hourly ozone at a variety of sites across southern California and makes the data publicly available (<http://www.arb.ca.gov/aqmis2/aqmis2.php>). Meteorological measurements at SCAQMD sites are made using RM Young Model 81000 Sonic Anemometers. TROPOMI level 2 tropospheric NO₂ (Copernicus Sentinel-5P (processed by ESA), 2021) columns and HCHO (European Space Agency, 2020) columns were obtained from the Goddard Earth Sciences Data and Information Services Center (GES DISC). The level 2 TROPOMI swath data are utilized at their native spatial resolution of 5.5x3.5 km without regridding for both species.



3 Results and Discussion

3.1 Comparisons with TROPOMI

To facilitate comparisons of the ground and satellite-based measurements, MAX-DOAS measurements were averaged over the hour surrounding the local overpass time ($\sim 13:30$ local time). To compensate for the MAX-DOAS measurements being path-averaged over multiple TROPOMI pixels, the TROPOMI pixel over Whittier and its nearest neighbors were averaged. The horizontal averaging of the MAX-DOAS varies over the study period due to its dependence on aerosol particle extinction in the lower troposphere. For this work, we assume a horizontal path length of ~ 10 km based on work by Irie et al. (2011). Error bars for the MAX-DOAS retrievals reflect propagated dSCD measurement errors and a priori error calculated using HEIPRO. Error bars for the TROPOMI observations reflect the spatial variability over the nearest neighbor pixels as calculated by the standard error of the mean. The resulting comparisons for both NO_2 and HCHO over the study period are shown in Fig. 3. The daily NO_2 measurements are generally well correlated ($R=0.73$), and monthly averages are even more well correlated ($R=0.89$), although the TROPOMI tropospheric column measurements are generally 14% lower than the ground-based NO_2 column measurements over this study. These results are consistent with other inter-comparisons of satellite and ground-based measurements (e.g. Jin et al., 2016; Wang et al., 2017; Pinardi et al., 2020; Chan et al., 2020; Ryan et al., 2023).

Formaldehyde measurements are less well correlated ($R=0.47$), although monthly averages are still well correlated ($R=0.82$). The comparison of this finding with prior comparisons is more muddled than that of NO_2 . TROPOMI HCHO columns retrieved are generally higher than those retrieved via MAX-DOAS over the course of the study. This discrepancy is in contrast to findings from some prior global studies (e.g. Chan et al., 2020; De Smedt et al., 2021), but are consistent with inter-comparisons done in polluted urban areas like London (Ryan et al., 2023) and Kinshasa (Yombo Phaka et al., 2023). There are times when TROPOMI retrieves large column densities that are not supported by ground based measurements. These events typically occur in the summer months and are potentially due to impacts of long range transport of wildfire plumes further aloft, which can complicate the retrieval of HCHO from satellite-based measurements (Zhao et al., 2022). It is also important to note that ground based MAX-DOAS retrievals, being most sensitive in the lowest 1-2 km of the atmosphere, do not represent the full tropospheric column which would be retrieved from a satellite based measurement.

3.2 Diurnal variations

Figure 5 shows diurnal cycles of the vertical distribution of both NO_2 and HCHO retrieved from MAX-DOAS observations. NO_2 vertical columns ranged between $1.2\text{e}15$ - $2.9\text{e}17$ molecules cm^{-2} with a median LT-VCD of $7.9\text{e}15$. Near surface mole fractions ranged from near zero to 52 nmol mol^{-1} with a median value of 4.8 nmol mol^{-1} . NO_2 vertical distributions tend to be more surface based events in the morning with peak near surface mole fractions occurring between 6 and 8 am local time (Fig. 5b) and peak LT-VCDs occurring closer to noon (Fig. 5a). The observed peak near surface mole fractions and LT-VCDs are generally lower than those seen in Kim et al. (2016) during the 2010 CalNex campaign at all times of day. This discrepancy could also reflect the fact that our observations include weekend observations which have lower NO_2 throughout the study period (Fig. 4), seasonal differences since CalNex took place during the summer and our observations encompass all seasons,

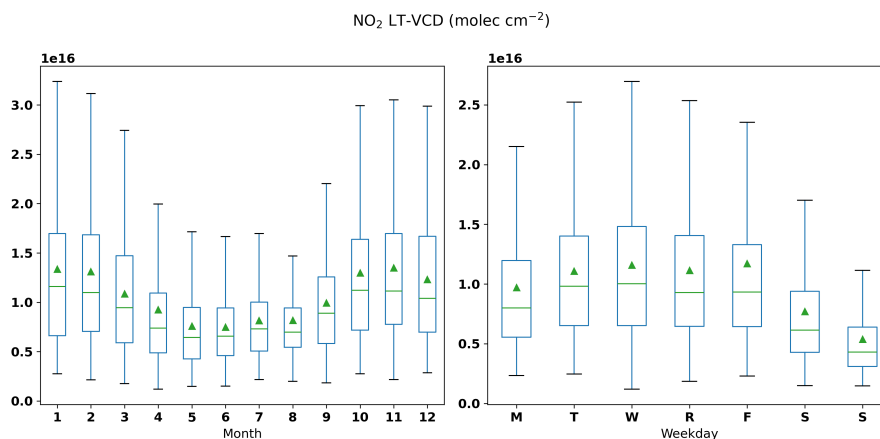


Figure 4. Box and whisker plots show the seasonal cycle for NO₂ LT-VCDs (left) and clear weekend effect (right). For both plots, the box encompasses the inner quartiles, the green line shows the median, the green triangle shows the mean, and the whiskers show the 5th to 95th percentile range.

ongoing local NO_x emission reductions (Duncan et al., 2016), or impacts of path averaging on MAX-DOAS retrievals. While
 140 CalNex took place in the summer and our data set spans all seasons, this is not a likely explanation as summer NO₂ LT-VCDs
 were typically lower than other months over the course of this study (Fig. 4). It should also be noted that our study period
 includes a time period encompassing COVID-19 related lockdown periods which likely altered local NO_x emissions. While
 our data set does not include observations prior to the lockdown period, work by Goldberg et al. (2020) shows TROPOMI NO₂
 columns decreased by 32.6% in the Los Angeles area from March 15th 2020 to April 30th 2020 after accounting for differences
 145 in meteorology and solar geometry. Our observed diurnal cycle shows NO₂ peaking for both quantities earlier in the day than
 observed by Kim et al. (2016), potentially due to differing local sources and traffic patterns in Whittier compared to Pasadena.
 The fraction of NO₂ retrieved in the lowest 200 m peaks in the early morning at approximately 40% before decreasing to
 around 20% in the late morning and staying there through the afternoon (Fig. 5c). The median retrieved f₂₀₀ was 26%. These
 dynamics are consistent with boundary layer dynamics typically observed in Southern California (Rahn and Mitchell, 2016).

150 In contrast, HCHO columns are consistently more vertically distributed with the fraction of HCHO at the surface being
 between 10 and 20% (Fig. 5c) with a median of 15%. HCHO LT-VCDs ranged between 1.6e15 to 9.7e16 molecules cm⁻² with
 a median LT-VCD of 6.4e15. Near surface mole fractions ranged from near zero to 14.9 nmol mol⁻¹ with a median value of
 1.9 nmol mol⁻¹. Retrieved near surface mole fractions also do not show any diurnal variability, with the median observations
 consistently being 2 nmol mol⁻¹ (Fig. 5b) throughout the day. In contrast, median formaldehyde LT-VCDs increase throughout
 155 the day peaking in the early afternoon (Fig. 5c), which has been seen in other HCHO column measurements (e.g. Ryan et al.,
 2020). Given the high temperatures and large amount of vegetation around the measurement site, it is likely this peak in HCHO
 can be at least partially attributed to biogenic sources (e.g. Kaiser et al., 2015; Zhao et al., 2022; Chen et al., 2023). This peak

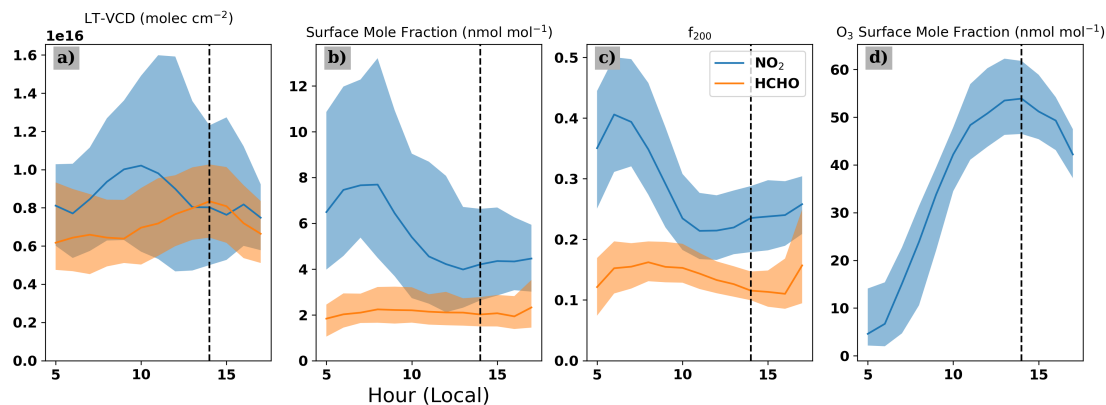


Figure 5. Plots show the median observed values (solid line) as well as the inner quartile range (shaded regions) for NO₂(blue) and HCHO (orange) binned by hour of the observation. From left to right the plots show, lower tropospheric vertical column density (a), near surface mole fraction (b), and the f_{200} , the fraction of the retrieved column in the lowest 200 m of the atmosphere (c). The median time of peak ozone mole fractions observed at the Pico Rivera CARB site is denoted with a vertical dashed line. Panel d shows the average diurnal ozone cycle over the study period.

in HCHO also coincides with the daily peak in median ozone mole fractions measured at the nearby California Air Resources Board site in Pico Rivera.

160 3.3 Examining Ozone Production Chemistry with MAX-DOAS

Ozone formation is dependent on both volatile organic compounds and nitrogen oxides (Sillman et al., 1990). Depending on the relative abundance of both quantities, ozone production can be characterized as NO_x limited, where reductions in NO_x emissions will be more effective limiting ozone formation, and NO_x saturated, where VOC emissions reductions will be more effective limiting ozone formation. Diagnosis of the ozone formation regime requires insights into the relative abundance of
 165 both VOCs and NO_x. To obtain this information from remote sensing measurements, formaldehyde and NO₂ retrievals can be used (e.g. Martin et al., 2004). FNR values are commonly derived from satellite based remote sensing measurements to provide insights on regional scale ozone production chemistry (e.g. Martin et al., 2004; Duncan et al., 2010; Jin et al., 2017, 2020; Souri et al., 2020). Comparisons of satellite based FNR with surface ozone mole fraction measurements enable the determination of FNR values indicating a transition between NO_x limited and NO_x saturated ozone production (e.g. Jin et al., 2020).

170 To estimate threshold FNR values from MAX-DOAS measurements, we paired hourly averaged MAX-DOAS observations with ozone measurement data from the Pico Rivera CARB site. We then calculated the probability of the observed ozone exceeding the United States ambient air quality standard of 70 nmol mol⁻¹ as a function of FNR using both near surface mole fractions and LT-VCD, both of which are retrieved concurrently. For each method, the maximum probability of an ozone exedence as a function of FNR and its associated uncertainty was determined using a 2nd order polynomial fit following
 175 methods described in Jin et al. (2020). Figure 6 shows FNR values derived from retrieved surface mole fractions are generally

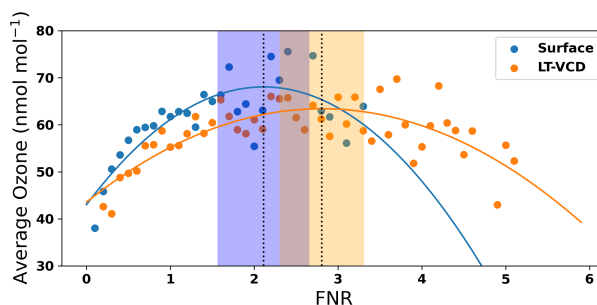


Figure 6. Determination of ozone formation regimes from ground-based MAX-DOAS data. Ozone values binned by surface FNR are shown in blue, while those binned by LT-VCD FNR are shown in orange. Second order polynomial fits are shown using solid lines, with the shaded region representing the uncertainty in the maximum value. Dashed vertical lines represent the maximum probability of an ozone exceedance as a function of FNR for both methods.

lower than those derived from LT-VCD measurements, although the transition ranges determined by the two techniques do overlap suggesting a general agreement of the two methods of determining the ozone production regime using ground-based remote sensing. The combination of ranges suggests the range of FNR values indicating a transition between NO_x limited and NO_x saturated ozone production in Whittier is between 1.6 and 3.3 (Fig. 6). Satellite based estimates of threshold values of this ratio that would indicate a transition in ozone formation chemistry regimes vary regionally but were found to be between 4 and 5 over the Los Angeles metropolitan area based on a study of 20 years of satellite-based FNR observations (Jin et al., 2020). The MAX-DOAS measurements in this study suggest this transition between production regimes occurs at a lower FNR in Whittier than observed over LA generally.

The differences between surface and column based FNR retrievals is most pronounced in the early morning and mid afternoon, reflecting the diurnal variability of the vertical profiles of NO₂ and HCHO (Fig. 7). Near surface ozone exceedances are more likely when HCHO is enhanced (Fig. 8), this leads to a disconnect between satellite based observations since HCHO profiles tend to have the bulk of the HCHO present aloft, away from the surface (Fig. 5). This variability in HCHO vertical distribution drives the deviation between surface-based and column based FNRs potentially indicating a misdiagnosis of ozone production regimes based on satellite based observations over Whittier as suggested in Schroeder et al. (2017) and reflected in the relatively poor agreement of FNRs between satellite and ground-based observations seen in this study (Fig. 3c). Large uncertainties in HCHO columns retrieved from TROPOMI (Fig. 3) likely also contribute to the poor agreement between TROPOMI and ground-based ratios as seen in Sourì et al. (2023). The interpretations of these ratios is also complicated by the impacts of NO_x on VOC oxidation which impacts the formation of HCHO and complicates the use of HCHO as a VOC proxy (Chan Miller et al., 2017). During the study period, we observe that increases in ozone exceedance probability are driven by enhancements in HCHO regardless of NO₂ amount (Fig. 8).

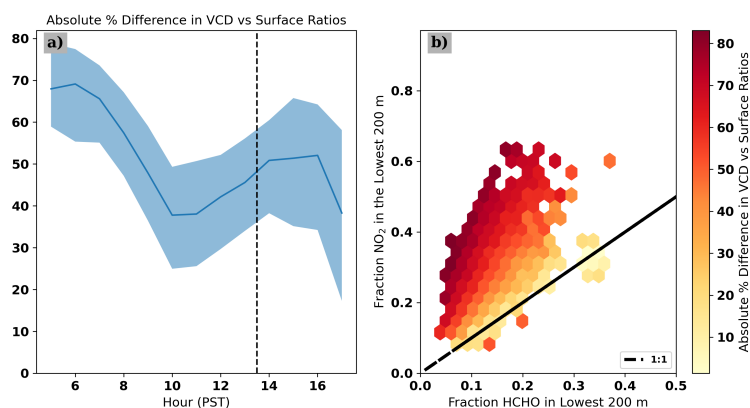


Figure 7. Panel a shows the diurnal variation of the FNR difference expressed as a percentage calculated using surface based quantities vs column based quantities. The solid line represents the median hourly observation and the shaded region represents the inner quartiles. The TROPOMI overpass time is denoted with a vertical dashed line. Panel b shows a hexagonally binned scatter plot of the distribution of FNR differences as a function of vertical distribution of ozone precursor. Each hexagon represents a bin, with color intensity indicating the average difference between the FNR near the surface and throughout the column within that region.

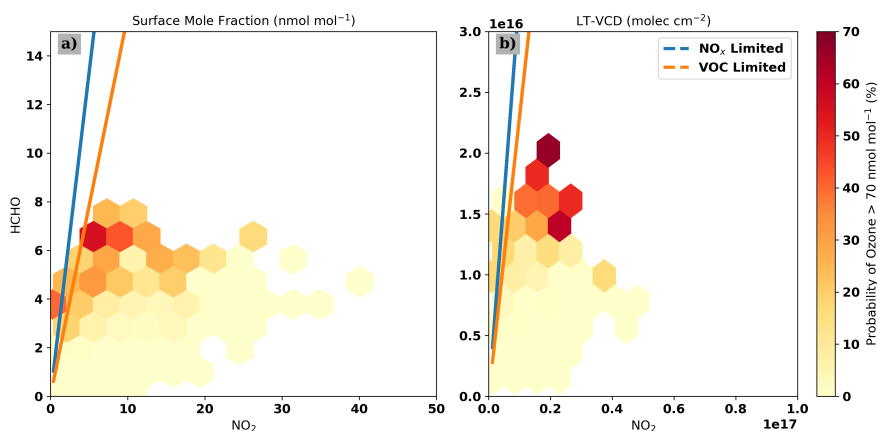


Figure 8. Panel a shows shows a hexagonally binned scatter plot of the probability of an ozone observation exceeding 70 nmol mol⁻¹ as a function of NO₂ and HCHO near surface mixing ratios. The blue and orange lines delineate NO_x limited and NO_x saturated regimes derived in Fig. 6. Panel a shows shows a hexagonally binned scatter plot of the probability of an ozone observation exceeding 70 nmol mol⁻¹ as a function of NO₂ and HCHO LT-VCDs. The blue and orange lines delineate NO_x limited and NO_x saturated regimes derived in Fig. 6.



4 Conclusions

For the first time, MAX-DOAS was used to retrieve the vertical distribution of ozone precursors NO_2 and HCHO over eastern Los Angeles. The retrieved LT-VCDs for NO_2 are well correlated with satellite based measurements from TROPOMI. Retrieved LT-VCDs for HCHO, while less well correlated than NO_2 are consistent with prior comparisons, and reinforce the need to improve HCHO retrievals from satellite based measurements. While the vertical distribution of NO_2 reflects increasing boundary layer height throughout the day, HCHO has a much more consistent vertical distribution with 80% of the column being present outside the lowest 200 m regardless of amount. These diurnal variations in both column and vertical profile complicate the interpretation of columns retrieved from geostationary satellite based observations. As an example the observed variability in vertical profiles can lead to differing diagnostics of ozone production via formaldehyde to NO_2 ratios. Using MAX-DOAS retrievals, FNRs can be derived from both near surface and column based quantities. Comparison of both methods to observed ozone yields similar transition values from a NO_x limited to NO_x saturated regimes, but the agreement between the two FNR varies considerably throughout the day, reflecting diurnal variations in both the column and vertical distribution of both precursor species. These findings point to the need to consider the vertical distribution of NO_2 and HCHO when interpreting FNRs derived from satellite based measurements to accurately diagnose ozone production chemistry using geostationary satellite observations, particularly in the late afternoon which has larger differences between surface and column based FNR and coincides with times when enhanced near surface ozone mole fractions associated with adverse impacts on human health are most prevalent.

Data availability. MAX-DOAS retrievals of NO_2 and HCHO lower tropospheric column densities and near surface mole fractions are available at <https://doi.org/10.5281/zenodo.11117573>(Peterson, 2024). Data from the Pico Rivera #2 surface monitoring station used in this paper are available at California Air Resource Board (CARB)'s Air Quality and Meteorological Information System (<http://www.arb.ca.gov/aqmis2/aqmis2.php>). Differential slant column densities are available from the corresponding author upon request.

Author contributions. PKP led data analysis, drafted the manuscript, and supervised all work done on the manuscript. EH and LT participated in data analysis. AD maintained the MAX-DOAS instrument during this study. All authors reviewed and contributed to the submitted manuscript.

Competing interests. The authors declare they have no competing interests.

Acknowledgements. E. Hernandez was partially supported by a Whittier College Don '50 and Virginia Baudrand Fellowship in Chemistry. The authors gratefully acknowledge Jochen Stutz for their efforts in establishing and maintaining the CalTech AERONET site, as well as

<https://doi.org/10.5194/egusphere-2024-1460>

Preprint. Discussion started: 27 August 2024

© Author(s) 2024. CC BY 4.0 License.



Alexei Rozanov from IUP Bremen for providing the SCIATRAN radiative transfer code which serves as the forward model for the HEIPRO retrieval code. PKP acknowledges support from the National Aeronautics and Space Administration (NASA) Earth Science Research Program (80NSSC22K1790)

225



References

- Chan, K. L., Wiegner, M., van Geffen, J., De Smedt, I., Alberti, C., Cheng, Z., Ye, S., and Wenig, M.: MAX-DOAS Measurements of Tropospheric NO₂ and HCHO in Munich and the Comparison to OMI and TROPOMI Satellite Observations, *Atmospheric Measurement Techniques*, 13, 4499–4520, <https://doi.org/10.5194/amt-13-4499-2020>, 2020.
- 230 Chan Miller, C., Jacob, D. J., Marais, E. A., Yu, K., Travis, K. R., Kim, P. S., Fisher, J. A., Zhu, L., Wolfe, G. M., Hanisco, T. F., Keutsch, F. N., Kaiser, J., Min, K. E., Brown, S. S., Washenfelder, R. A., González Abad, G., and Chance, K.: Glyoxal Yield from Isoprene Oxidation and Relation to Formaldehyde: Chemical Mechanism, Constraints from SENEX Aircraft Observations, and Interpretation of OMI Satellite Data, *Atmospheric Chemistry and Physics*, 17, 8725–8738, <https://doi.org/10.5194/acp-17-8725-2017>, 2017.
- Chen, Y., Liu, C., Su, W., Hu, Q., Zhang, C., Liu, H., and Yin, H.: Identification of Volatile Organic Compound Emissions from Anthro-
235 pogenic and Biogenic Sources Based on Satellite Observation of Formaldehyde and Glyoxal, *Science of The Total Environment*, 859, 159997, <https://doi.org/10.1016/j.scitotenv.2022.159997>, 2023.
- Copernicus Sentinel-5P (processed by ESA): Copernicus Sentinel Data Processed by ESA, Koninklijk Nederlands Meteorologisch Instituut (KNMI) (2021), GES DISC Dataset: Sentinel-5P TROPOMI Tropospheric NO₂ 1-Orbit L2 5.5km x 3.5km (S5P_L2_NO2_HiR 2), <https://doi.org/10.5270/S5P-9bnp8q8>, 2021.
- 240 De Smedt, I., Pinardi, G., Vigouroux, C., Compernelle, S., Bais, A., Benavent, N., Boersma, F., Chan, K.-L., Donner, S., Eichmann, K.-U., Hedelt, P., Hendrick, F., Irie, H., Kumar, V., Lambert, J.-C., Langerock, B., Lerot, C., Liu, C., Loyola, D., Piters, A., Richter, A., Rivera Cárdenas, C., Romahn, F., Ryan, R. G., Sinha, V., Theys, N., Vlietinck, J., Wagner, T., Wang, T., Yu, H., and Van Roozendael, M.: Comparative Assessment of TROPOMI and OMI Formaldehyde Observations and Validation against MAX-DOAS Network Column Measurements, *Atmospheric Chemistry and Physics*, 21, 12 561–12 593, <https://doi.org/10.5194/acp-21-12561-2021>, 2021.
- 245 Duncan, B. N., Yoshida, Y., Olson, J. R., Sillman, S., Martin, R. V., Lamsal, L., Hu, Y., Pickering, K. E., Retscher, C., Allen, D. J., and Crawford, J. H.: Application of OMI Observations to a Space-Based Indicator of NO_x and VOC Controls on Surface Ozone Formation, *Atmospheric Environment*, 44, 2213–2223, <https://doi.org/10.1016/j.atmosenv.2010.03.010>, 2010.
- Duncan, B. N., Lamsal, L. N., Thompson, A. M., Yoshida, Y., Lu, Z., Streets, D. G., Hurwitz, M. M., and Pickering, K. E.: A Space-Based, High-Resolution View of Notable Changes in Urban NO_x Pollution around the World (2005–2014), *Journal of Geophysical Research: Atmospheres*, 121, 976–996, <https://doi.org/10.1002/2015JD024121>, 2016.
- 250 Esri: World Imagery - Overview, <https://www.arcgis.com/home/item.html?id=10df2279f9684e4a9f6a7f08febac2a9>, 2024.
- European Space Agency: TROPOMI Level 2 Formaldehyde, <https://doi.org/10.5270/S5P-vg1i7t0>, 2020.
- Fayt, C., De Smedt, I., Letocart, V., Merlaud, A., Pinardi, G., Van Roozendael, M., and Roozendael, M. V. A. N.: QDOAS Software User Manual, Belgian Institute for Space Aeronomy, 2011.
- 255 Frieß, U., Monks, P. S., Remedios, J. J., Rozanov, A., Sinreich, R., Wagner, T., and Platt, U.: MAX-DOAS O₄ Measurements: A New Technique to Derive Information on Atmospheric Aerosols: 2. Modeling Studies, *Journal of Geophysical Research*, 111, D14 203, <https://doi.org/10.1029/2005JD006618>, 2006.
- Goldberg, D. L., Anenberg, S. C., Griffin, D., McLinden, C. A., Lu, Z., and Streets, D. G.: Disentangling the Impact of the COVID-19 Lockdowns on Urban NO₂ from Natural Variability, *Geophysical Research Letters*, <https://doi.org/10.1029/2020GL089269>, 2020.
- 260 Haagen-Smit, A. J.: Chemistry and Physiology of Los Angeles Smog, *Industrial & Engineering Chemistry*, 44, 1342–1346, <https://doi.org/10.1021/ie50510a045>, 1952.



- Hering, S. V. and Blumenthal, D. L.: Southern California Air Quality Study (SCAQ5) Description of Measurement Activities. Final Report, 1989.
- Hönninger, G., von Friedeburg, C., and Platt, U.: Multi Axis Differential Optical Absorption Spectroscopy (MAX-DOAS), *Atmospheric Chemistry and Physics*, 4, 231–254, <https://doi.org/10.5194/acp-4-231-2004>, 2004.
- Irie, H., Takashima, H., Kanaya, Y., Boersma, K. F., Gast, L., Wittrock, F., Brunner, D., Zhou, Y., and Van Roozendaal, M.: Eight-Component Retrievals from Ground-Based MAX-DOAS Observations, *Atmospheric Measurement Techniques*, 4, 1027–1044, <https://doi.org/10.5194/amt-4-1027-2011>, 2011.
- Jacob, D. J., Crawford, J. H., Maring, H., Clarke, A. D., Dibb, J. E., Emmons, L. K., a. Ferrare, R., a. Hostetler, C., Russell, P. B., Singh, H. B., Thompson, a. M., Shaw, G. E., McCauley, E., Pederson, J. R., and a. Fisher, J.: The Arctic Research of the Composition of the Troposphere from Aircraft and Satellites (ARCTAS) Mission: Design, Execution, and First Results, *Atmospheric Chemistry and Physics*, 10, 5191–5212, <https://doi.org/10.5194/acp-10-5191-2010>, 2010.
- Jin, J., Ma, J., Lin, W., Zhao, H., Shaiganfar, R., Beirle, S., and Wagner, T.: MAX-DOAS Measurements and Satellite Validation of Tropospheric NO₂ and SO₂ Vertical Column Densities at a Rural Site of North China, *Atmospheric Environment*, 133, 12–25, <https://doi.org/10.1016/j.atmosenv.2016.03.031>, 2016.
- Jin, X., Fiore, A. M., Murray, L. T., Valin, L. C., Lamsal, L. N., Duncan, B., Folkert Boersma, K., De Smedt, I., Abad, G. G., Chance, K., and Tonnesen, G. S.: Evaluating a Space-Based Indicator of Surface Ozone-NO_x-VOC Sensitivity Over Midlatitude Source Regions and Application to Decadal Trends, *Journal of Geophysical Research: Atmospheres*, 122, 10 439–10 461, <https://doi.org/10.1002/2017JD026720>, 2017.
- Jin, X., Fiore, A., Boersma, K. F., De Smedt, I., and Valin, L.: Inferring Changes in Summertime Surface Ozone-NO_x-VOC Chemistry over U.S. Urban Areas from Two Decades of Satellite and Ground-Based Observations, *Environmental Science & Technology*, p. acs.est.9b07785, <https://doi.org/10.1021/acs.est.9b07785>, 2020.
- Kaiser, J., Wolfe, G. M., Min, K. E., Brown, S. S., Miller, C. C., Jacob, D. J., deGouw, J. A., Graus, M., Hanisco, T. F., Holloway, J., Peischl, J., Pollack, I. B., Ryerson, T. B., Warneke, C., Washenfelder, R. A., and Keutsch, F. N.: Reassessing the Ratio of Glyoxal to Formaldehyde as an Indicator of Hydrocarbon Precursor Speciation, *Atmospheric Chemistry and Physics*, 15, 7571–7583, <https://doi.org/10.5194/acp-15-7571-2015>, 2015.
- Kim, K., Yabushita, A., Okumura, M., Saiz-Lopez, A., Cuevas, C. A., Blaszcak-Boxe, C. S., Min, D. W., Yoon, H.-I., and Choi, W.: Production of Molecular Iodine and Tri-iodide in the Frozen Solution of Iodide: Implication for Polar Atmosphere, *Environmental Science & Technology*, 50, 1280–1287, <https://doi.org/10.1021/acs.est.5b05148>, 2016.
- Kreher, K., Van Roozendaal, M., Hendrick, F., Apituley, A., Dimitropoulou, E., Frieß, U., Richter, A., Wagner, T., Lampel, J., Abuhassan, N., Ang, L., Anguas, M., Bais, A., Benavent, N., Bösch, T., Bognar, K., Borovski, A., Bruchkouski, I., Cede, A., Chan, K. L., Donner, S., Drosoglou, T., Fayt, C., Finkenzeller, H., Garcia-Nieto, D., Gielen, C., Gómez-Martín, L., Hao, N., Henzing, B., Herman, J. R., Hermans, C., Hoque, S., Irie, H., Jin, J., Johnston, P., Khayyam Butt, J., Khokhar, F., Koenig, T. K., Kuhn, J., Kumar, V., Liu, C., Ma, J., Merlaud, A., Mishra, A. K., Müller, M., Navarro-Comas, M., Ostendorf, M., Pazmino, A., Peters, E., Pinardi, G., Pinharanda, M., PETERS, A., Platt, U., Postlyakov, O., Prados-Roman, C., Puentedura, O., Querel, R., Saiz-Lopez, A., Schönhardt, A., Schreier, S. F., Seyler, A., Sinha, V., Spinei, E., Strong, K., Tack, F., Tian, X., Tiefengraber, M., Tirpitz, J.-L., van Gent, J., Volkamer, R., Vrekoussis, M., Wang, S., Wang, Z., Wenig, M., Wittrock, F., Xie, P. H., Xu, J., Yela, M., Zhang, C., and Zhao, X.: Intercomparison of NO₂, O₄, O₃ and HCHO Slant Column Measurements by MAX-DOAS and Zenith-Sky UV-visible Spectrometers During, *Atmospheric Measurement Techniques*, 13, 2169–2208, <https://doi.org/10.5194/amt-13-2169-2020>, 2020.



- 300 Martin, R. V., Fiore, A. M., and Van Donkelaar, A.: Space-Based Diagnosis of Surface Ozone Sensitivity to Anthropogenic Emissions, *Geophysical Research Letters*, 31, n/a–n/a, <https://doi.org/10.1029/2004GL019416>, 2004.
- Millet, D. B., Jacob, D. J., Turquety, S., Hudman, R. C., Wu, S., Fried, A., Walega, J., Heikes, B. G., Blake, D. R., Singh, H. B., Anderson, B. E., and Clarke, A. D.: Formaldehyde Distribution over North America: Implications for Satellite Retrievals of Formaldehyde Columns and Isoprene Emission, *Journal of Geophysical Research: Atmospheres*, 111, <https://doi.org/10.1029/2005JD006853>, 2006.
- 305 Nussbaumer, C. M., Place, B. K., Zhu, Q., Pfannerstill, E. Y., Wooldridge, P., Schulze, B. C., Arata, C., Ward, R., Bucholtz, A., Seinfeld, J. H., Goldstein, A. H., and Cohen, R. C.: Measurement Report: Airborne Measurements of NO_x Fluxes over Los Angeles during the RECAP-CA 2021 Campaign, *Atmospheric Chemistry and Physics*, 23, 13 015–13 028, <https://doi.org/10.5194/acp-23-13015-2023>, 2023.
- Payne, V. H., Clough, S. A., Shephard, M. W., Nassar, R., and Logan, J. A.: Information-Centered Representation of Retrievals with Limited Degrees of Freedom for Signal: Application to Methane from the Tropospheric Emission Spectrometer, *Journal of Geophysical Research*, 310, D10 307, <https://doi.org/10.1029/2008JD010155>, 2009.
- Peterson, P. K.: Whittier_CH2O_NO2_MAXDOAS_20200326, <https://doi.org/10.5281/zenodo.11117573>, 2024.
- Peterson, P. K., Simpson, W. R., Pratt, K. A., Shepson, P. B., Frieß, U., Zielcke, J., Platt, U., Walsh, S. J., and Nghiem, S. V.: Dependence of the Vertical Distribution of Bromine Monoxide in the Lower Troposphere on Meteorological Factors Such as Wind Speed and Stability, *Atmospheric Chemistry and Physics*, 15, <https://doi.org/10.5194/acp-15-2119-2015>, 2015.
- 315 Pinardi, G., Van Roozendaal, M., Hendrick, F., Theys, N., Abuhassan, N., Bais, A., Boersma, F., Cede, A., Chong, J., Donner, S., Drosoglou, T., Frieß, U., Granville, J., Herman, J., Eskes, H., Holla, R., Hovila, J., Irie, H., Kanaya, Y., Karagkiozidis, D., Kouremeti, N., Lambert, J.-C., Ma, J., Peters, E., Peters, A., Postlyakov, O., Richter, A., Remmers, J., Takashima, H., Tiefengraber, M., Valks, P., Vlemmix, T., Wagner, T., and Wittrock, F.: Validation of Tropospheric NO₂ Column Measurements of GOME-2A and OMI Using MAX-DOAS and Direct Sun Network Observations, *Atmospheric Measurement Techniques Discussions*, pp. 1–55, <https://doi.org/10.5194/amt-2020-76>, 320 2020.
- Pusede, S. E., Steiner, A. L., and Cohen, R. C.: Temperature and Recent Trends in the Chemistry of Continental Surface Ozone, *Chemical Reviews*, 115, 3898–3918, <https://doi.org/10.1021/cr5006815>, 2015.
- Rahn, D. A. and Mitchell, C. J.: Diurnal Climatology of the Boundary Layer in Southern California Using AMDAR Temperature and Wind Profiles, *Journal of Applied Meteorology and Climatology*, 55, 1123–1137, <https://doi.org/10.1175/JAMC-D-15-0234.1>, 2016.
- 325 Rodgers, C. D.: *Inverse Methods For Atmospheric Sounding: Theory and Practice*, World Scientific, Singapore, 2000.
- Rozanov, a., Rozanov, V., Buchwitz, M., Kokhanovsky, a., and Burrows, J. P.: SCIATRAN 2.0 - A New Radiative Transfer Model for Geophysical Applications in the 175-2400 Nm Spectral Region, *Advances in Space Research*, 36, 1015–1019, <https://doi.org/10.1016/j.asr.2005.03.012>, 2005.
- Ryan, R. G., Rhodes, S., Tully, M., and Schofield, R.: Surface Ozone Exceedances in Melbourne, Australia Are Shown to Be under NO_x Control, as Demonstrated Using Formaldehyde:NO₂ and Glyoxal:Formaldehyde Ratios, *Science of The Total Environment*, 749, 141 460, <https://doi.org/10.1016/j.scitotenv.2020.141460>, 2020.
- 330 Ryan, R. G., Marais, E. A., Gershenson-Smith, E., Ramsay, R., Muller, J.-P., Tirpitz, J.-L., and Frieß, U.: Measurement Report: MAX-DOAS Measurements Characterise Central London Ozone Pollution Episodes during 2022 Heatwaves, *Atmospheric Chemistry and Physics*, 23, 7121–7139, <https://doi.org/10.5194/acp-23-7121-2023>, 2023.
- 335 Ryerson, T. B., Andrews, A. E., Angevine, W. M., Bates, T. S., Brock, C. A., Cairns, B., Cohen, R. C., Cooper, O. R., De Gouw, J. A., Fehsenfeld, F. C., Ferrare, R. A., Fischer, M. L., Flagan, R. C., Goldstein, A. H., Hair, J. W., Hardesty, R. M., Hostetler, C. A., Jimenez, J. L., Langford, A. O., McCauley, E., McKeen, S. A., Molina, L. T., Nenes, A., Oltmans, S. J., Parrish, D. D., Pederson, J. R., Pierce,



- R. B., Prather, K., Quinn, P. K., Seinfeld, J. H., Senff, C. J., Sorooshian, A., Stutz, J., Surratt, J. D., Trainer, M., Volkamer, R., Williams, E. J., and Wofsy, S. C.: The 2010 California Research at the Nexus of Air Quality and Climate Change (CalNex) Field Study, *Journal of Geophysical Research Atmospheres*, 118, 5830–5866, <https://doi.org/10.1002/jgrd.50331>, 2013.
- Schroeder, J. R., Crawford, J. H., Fried, A., Walega, J., Weinheimer, A., Wisthaler, A., Müller, M., Mikoviny, T., Chen, G., Shook, M., Blake, D. R., and Tonnesen, G. S.: New Insights into the Column CH₂O/NO₂ Ratio as an Indicator of near-Surface Ozone Sensitivity, *Journal of Geophysical Research: Atmospheres*, 122, 8885–8907, <https://doi.org/10.1002/2017JD026781>, 2017.
- Sillman, S., Logan, J. A., and Wofsy, S. C.: The Sensitivity of Ozone to Nitrogen Oxides and Hydrocarbons in Regional Ozone Episodes, *Journal of Geophysical Research*, 95, 1837, <https://doi.org/10.1029/JD095iD02p01837>, 1990.
- Souri, A. H., Nowlan, C. R., Wolfe, G. M., Lamsal, L. N., Chan Miller, C. E., Abad, G. G., Janz, S. J., Fried, A., Blake, D. R., Weinheimer, A. J., Diskin, G. S., Liu, X., and Chance, K.: Revisiting the Effectiveness of HCHO/NO₂ Ratios for Inferring Ozone Sensitivity to Its Precursors Using High Resolution Airborne Remote Sensing Observations in a High Ozone Episode during the KORUS-AQ Campaign, *Atmospheric Environment*, 224, 117 341, <https://doi.org/10.1016/j.atmosenv.2020.117341>, 2020.
- Souri, A. H., Johnson, M. S., Wolfe, G. M., Crawford, J. H., Fried, A., Wisthaler, A., Brune, W. H., Blake, D. R., Weinheimer, A. J., Verhoelst, T., Compornolle, S., Pinardi, G., Vigouroux, C., Langerock, B., Choi, S., Lamsal, L., Zhu, L., Sun, S., Cohen, R. C., Min, K.-E., Cho, C., Philip, S., Liu, X., and Chance, K.: Characterization of Errors in Satellite-Based HCHO & NO₂ Tropospheric Column Ratios with Respect to Chemistry, Column-to-PBL Translation, Spatial Representation, and Retrieval Uncertainties, *Atmospheric Chemistry and Physics*, 23, 1963–1986, <https://doi.org/10.5194/acp-23-1963-2023>, 2023.
- Thompson, J. E., Hayes, P. L., Jimenez, J. L., Adachi, K., Zhang, X., Liu, J., Weber, R. J., and Buseck, P. R.: Aerosol Optical Properties at Pasadena, CA during CalNex 2010, *Atmospheric Environment*, 55, 190–200, <https://doi.org/10.1016/j.atmosenv.2012.03.011>, 2012.
- Wagner, T., Dix, B., Friedeburg, C. V., Frieß, U., Sanghavi, S., Sinreich, R., and Platt, U.: MAX-DOAS O₄ Measurements: A New Technique to Derive Information on Atmospheric Aerosols-Principles and Information Content, *Journal of Geophysical Research: Atmospheres*, 109, n/a–n/a, <https://doi.org/10.1029/2004JD004904>, 2004.
- Wagner, T., Beirle, S., Remmers, J., Shaiganfar, R., and Wang, Y.: Absolute Calibration of the Colour Index and O₄ Absorption Derived from Multi AXis (MAX-)DOAS Measurements and Their Application to a Standardised Cloud Classification Algorithm, *Atmospheric Measurement Techniques*, 9, 4803–4823, <https://doi.org/10.5194/amt-9-4803-2016>, 2016.
- Wang, Y., Lampel, J., Xie, P., Beirle, S., Li, A., Wu, D., and Wagner, T.: Ground-Based MAX-DOAS Observations of Tropospheric Aerosols, NO₂, SO₂ and HCHO in Wuxi, China, from 2011 to 2014, *Atmospheric Chemistry and Physics*, 17, 2189–2215, <https://doi.org/10.5194/acp-17-2189-2017>, 2017.
- Warneke, C., Veres, P., Holloway, J. S., Stutz, J., Tsai, C., Alvarez, S., Rappenglueck, B., Fehsenfeld, F. C., Graus, M., Gilman, J. B., and de Gouw, J. A.: Airborne Formaldehyde Measurements Using PTR-MS: Calibration, Humidity Dependence, Inter-Comparison and Initial Results, *Atmospheric Measurement Techniques*, 4, 2345–2358, <https://doi.org/10.5194/amt-4-2345-2011>, 2011.
- Yilmaz, S.: Retrieval of Atmospheric Aerosol and Trace Gas Vertical Profiles Using Multi-Axis Differential Optical Absorption Spectroscopy, Ph.D. thesis, University of Heidelberg, 2012.
- Yombo Phaka, R., Merlaud, A., Pinardi, G., Friedrich, M. M., Van Roozendaal, M., Müller, J.-F., Stavrou, T., De Smedt, I., Hendrick, F., Dimitropoulou, E., Bopili Mbotia Lepiba, R., Phuku Phuati, E., Djibi, B. L., Jacobs, L., Fayt, C., Mbungu Tsumbu, J.-P., and Mahieu, E.: Ground-Based Multi-AXis Differential Optical Absorption Spectroscopy (MAX-DOAS) Observations of NO₂ and H₂CO at Kinshasa



375 and Comparisons with TROPOMI Observations, *Atmospheric Measurement Techniques*, 16, 5029–5050, <https://doi.org/10.5194/amt-16-5029-2023>, 2023.

Zhao, T., Mao, J., Simpson, W. R., De Smedt, I., Zhu, L., Hanisco, T. F., Wolfe, G. M., St. Clair, J. M., González Abad, G., Nowlan, C. R., Barletta, B., Meinardi, S., Blake, D. R., Apel, E. C., and Hornbrook, R. S.: Source and Variability of Formaldehyde (HCHO) at Northern High Latitudes: An Integrated Satellite, Aircraft, and Model Study, *Atmospheric Chemistry and Physics*, 22, 7163–7178,

380 <https://doi.org/10.5194/acp-22-7163-2022>, 2022.